Received: 6 January 2022 | Revised: 21 September 2022 | Accepted: 22 September 2022

DOI: 10.1111/ejss.13311

ORIGINAL ARTICLE

European Journal of Soil Science WILEY

Factors controlling SOC stability in colluvial soils under contrasting climate and soil weathering conditions

Pengzhi Zhao[1] | **Sebastian Doetterl**[2] | **Zhengang Wang**[3] | **Alison M. Hoyt**[4] | **Enheng Wang**[5] | **Hanqing Yu**[6] | **Laura Quijano**[1] | **Daniel J. Fallu**[7] | **Antony G. Brown**[7] | **Johan Six**[8] | **Kristof Van Oost**[1]

[1]Georges Lemaître Centre for Earth and Climate Research, Earth and Life Institute, Louvain-la-Neuve, Belgium

[2]Soil Resources Group, Department of Environmental System Science, ETH Zurich, Zürich, Switzerland

[3]Key Laboratory of Urbanization and Geosimulation of Guangdong Province, School of Geography and Planning, Sun Yat-sen University, Guangzhou, China

[4]Department of Biogeochemical Processes, Max Planck Institute for Biogeochemistry, Jena, Germany

[5]College of Forestry, Northeast Forestry University, Harbin, China

[6]Institute of Environment and Sustainable Development in Agriculture, Chinese Academy of Agricultural Sciences, Beijing, China

[7]Tromsø University Museum, UiT The Arctic University of Norway, Tromsø, Norway

[8]Sustainable Agroecosystems Group, Department of Environmental System Science, ETH Zurich, Zürich, Switzerland

Correspondence
Pengzhi Zhao, Georges Lemaître Centre for Earth and Climate Research, Earth and Life Institute, UCLouvain, Louvain-la-Neuve 1348, Belgium.
Email: pengzhi.zhao@outlook.com

Funding information
China Scholarship Council, Grant/Award Number: 201706600009; H2020 European Research Council, Grant/Award Numbers: 695101, 787790

Abstract

Although agricultural colluvial soils are important storage for soil organic carbon (SOC), the mechanisms underlying colluvial (cumulative soils) SOC stability have received little attention so far. In this study, we aim to understand to what extent the main controls on colluvial SOC stability differ from those observed in non-colluvial soils. Paired soil profiles (non-colluvial versus colluvial) were collected from five sites which differ in climate, soil geochemical background and cultivation history. Topsoil (0–10 cm) and subsoil (30–50 cm) were analysed for SOC fractions, mineral composition, potential soil respiration and radiocarbon content. Our analysis showed that for non-colluvial soils, climate, cultivation history and weathering degree have significant effects on potential soil respiration. In contrast, for colluvial soils, the most influential factor for potential soil respiration was the rate of accretion and this was independent of climatic and geochemical context. Furthermore, accretion rates indirectly affected potential soil respiration by interacting with the degree of weathering of deposited soil. This changed the mineral matrix of colluvial soil settings and thereby may enhance soil mineral-related SOC stabilisation mechanisms. Together, these results suggest that the dominant controls on SOC stability in colluvial soils differ from those in non-colluvial soils, and the soil accretion rate is the most important control on colluvial SOC stability in agricultural systems.

Highlights

- The dominant controls on SOC stability in colluvial and non-colluvial soils were compared.

- Climate and mineral weathering predominantly control SOC stability in non-colluvial soils.
- In contrast, the accretion rate is the key factor controlling colluvial SOC stability.
- Accretion rate drives the role of mineral weathering in colluvial SOC stability.

KEYWORDS
carbon cycling, carbon sequestration, cultivation, soil erosion, stabilisation mechanism

1 | INTRODUCTION

Over the past decades, substantial progress has been made in understanding the mechanisms controlling soil organic carbon (SOC) stabilisation versus loss. Climate, soil geochemistry and human activities (e.g., cultivation) have been identified as dominant controls on SOC dynamics. However, most of this understanding is informed by studies conducted on level or low-gradient, stable landscapes (Carvalhais et al., 2014; Doetterl, Stevens, et al., 2015; Wang et al., 2019). Whether this knowledge can be simply transferred to colluvial soils in eroding landscapes is questionable and has been less addressed (e.g., Wang et al., 2018). Previous work has highlighted that erosion-induced changes in the soil geochemical matrix have important implications for colluvial SOC stabilisation (Berhe et al., 2012; Doetterl, Cornelis, et al., 2015). However, to what extent this link is influenced by climatic and mineral weathering controls is rarely considered. The importance of understanding the main controls on colluvial SOC stabilisation is further emphasised by the large amounts of SOC in colluvial stores. Since 1850, the expansion of agriculture has mobilised an estimated 63 ± 19 Pg C globally (Wang et al., 2017), of which 16 to 21 Pg C have been deposited in agricultural colluvial soils during the last 50 years (Van Oost et al., 2007). This makes agricultural colluvial soils as an important, yet underappreciated storage for SOC.

At the continental scale, the climate is generally considered to be the dominant control over SOC dynamics, as it often explains the largest proportion of variation in SOC turnover rates. On one hand, climate determines the C inputs into soils via its control of net primary production (Luo et al., 2017; Tang & Riley, 2015). On the other hand, climate (e.g., temperature) can greatly influence the soil microbial activity and thus SOC turnover, resulting in a clear dependence of SOC turnover time on temperature (Carvalhais et al., 2014; Feng et al., 2017). Hence, these SOC–temperature relations have been adopted in ecosystem C cycle models and Earth system models to predict the global C budget (Carvalhais et al., 2014). Although the precipitation is a relatively weaker predictor of total OC content compared to temperature (Doetterl, Stevens, et al., 2015; Luo et al., 2017), it has been suggested that soil effective moisture (precipitation after subtracting potential evapotranspiration) strongly controls the fraction of SOC retained by reactive minerals across diverse parent materials and biomes (Kramer & Chadwick, 2018). This is mainly due to the soil water balance causing nonlinear changes in many soil properties, including soil pH, nutrient supply, and weathering degree that are likely to determine C stability (Kramer & Chadwick, 2018). At the regional scale, the climate becomes less important and soil geochemical properties have a larger influence on SOC stabilisation (e.g., Doetterl, Stevens, et al., 2015; Viscarra Rossel et al., 2019). Soil geochemical properties, resulting from climate and vegetation controls on mineral weathering of varying soil parent material, determine the availability of reactive mineral surfaces and sorbents for forming soil aggregates and organo-mineral associations, which can protect SOC from decomposition for decades to centuries or even millennia (Denef & Six, 2005; Masiello et al., 2004). Under similar climatic conditions, differences in the geochemistry and weathering susceptibility of parent material can result in distinct soil geochemical properties and hence SOC stabilisation mechanisms (Blume et al., 2016). At the smaller plot and slope scale, geomorphic processes can have important implications for SOC stabilisation. For example, erosion processes break down macroaggregates and expose formerly enclosed SOC to decomposers (Six et al., 2008). This facilitates oxidation and hydration of the previously protected SOC, enhancing its mineralization (Six et al., 2008; Wang, Cammeraat, et al., 2014). In addition, erosion can preferentially transport finer soil particles together with clay minerals and reactive mineral oxides to colluvial environments (Berhe et al., 2012; Doetterl, Cornelis, et al., 2015; Zhao et al., 2022), providing colluvial soils with increased potential to physico–chemically

protect SOC against mineralization. Topography also exerts a control on soil hydrologic conditions via water flow and therefore interacts with mineral weathering and net primary productivity (NPP) (e.g., Metzen et al., 2019). This hydrologic mechanism is important for colluvial soils, which are typically located in valleys or concave slope positions (e.g., Wiaux et al., 2015) and can have significant horizontal components to throughflow and groundwater fluxes. However, to our knowledge, few studies have explicitly addressed the controls on colluvial SOC turnover for a range of environmental settings.

In this study, we contribute to this knowledge gap by presenting a study of SOC stabilisation in colluvial soils in five contrasting climatic and geochemical settings. Detailed soil geochemical properties (e.g., reactive mineral phases, exchangeable cations) and soil clay mineralogy composition were measured to explain the underlying mechanisms. We hypothesized that small-scale controls on colluvial C turnover such as selective deposition, aggregate breakdown and specific environmental conditions interact with large-scale controls such as climate, geochemistry and the duration of cultivation. The main objectives of this study were thus (i) to identify the dominant controls on colluvial SOC stability under different climate and mineral weathering settings, and (ii) to assess to what extent these controlling factors differ from those in stable, non-eroding soils.

2 | MATERIALS AND METHODS

2.1 | Study sites

We selected 20 samples from five coupled non-colluvial/colluvial sites spanning a large climatic (from arid to tropical) and soil geochemical range (Table 1). The accretion rates were quantified using tracer methods (see below). Site 1 (SP) is located in Northeastern Spain and is characterised by a high carbonate content (soil inorganic C ~ 5.4%) and a silty texture (mean 58%) with a relatively low sand content (29%) (Calcisols). Site 1 has been cultivated since the early 20th century (~120 years) and the main crops are winter wheat (Lizaga et al., 2018). Site 2 (NC) is located on the Chinese Loess (Cambisols); Soils are loess derived and have a very high silt content (~80%). The study area has a long history of cultivation dating back to c. 1500 years (> 1000 years), with wheat and corn as the major currently planted crops (Li et al., 2015). Site 3 (BE) is located in the Belgian loam belt (Luvisols). Here, agriculture can be traced back from the Iron Age to Medieval Period (c. 2300–300 BP) and at present, cereals, sugar beet and maize are cultivated. Site 4 (SC) is located in Yingde city, Guangdong province of South China. Soils are Ferralsols with a high silt (~55%) and sand content (~30%) (Liu et al., 2007). Human activities including deforestation and agriculture on steep slopes are the main reasons for the severe soil erosion in the area. Cereals are the current main crops. The study area has a relatively short history of agriculture (<80 years). Finally, site 5 (SB) is located at Arvorezinha catchment in the state of Rio Grande do Sul in South Brazil. The dominant soil type is Acrisols with a high silt (~65%) and clay content (~23%). The study area has a history of agriculture dating back to around 1925 (~95 years), and tobacco, corn, soybean and wheat are the dominant crops. Profile-specific accretion rates were derived from published estimates based on caesium-137 (^{137}Cs) measurements (Wang, Van Oost, et al., 2014 (BE); Li et al., 2015 (NC); Quijano et al., 2016 (SP); Minella et al., 2012 (SB); Zhang et al., 2011 (SC)). The ^{137}Cs activities were measured on the same cores used in this study, except for SC, where accretion rates were inferred from an erosion study in a nearby field with a similar topography and cultivation history (Zhang et al., 2011). The sites can be categorised into Mediterranean climate (Csa) (SP), semiarid continental climate (Bsk) (NC), temperate climate (Cfb) (BE) and subtropical climate (Cfa) (SC and SB) regions by considering climatic metrics such as the mean annual precipitation (MAP), mean annual temperature (MAT) and potential evapotranspiration (PET) (Table 1). Pedogenic Fe oxides (Fe_d/Fe_t) are indicative of the weathering status (Arduino et al., 1986) and we use this metric to describe the differences in weathering degree among the selected study sites.

2.2 | Field sampling and sample processing

Two replicates soil cores at each site were collected from relatively flat areas at the hilltop plateau which can be assumed to represent stable conditions (henceforth, non-colluvial soils) where no or little erosion or deposition has taken place. Soil cores were also collected from colluvial soils in concave landscape positions at each site as two replicates. Cores were taken using a pneumatic corer and soil samples were stored in sealed PVC tubes. Compaction occurring during coring, which was in the order of 3 to 8%, was corrected by linear extension of the length of the obtained soil column to the measured depth of the soil core-hole. Soil cores were cut at 5 cm intervals to a depth of 50 cm, air-dried (<30°C), and dry-sieved at 8 mm. Replicates soil cores were combined to make a composite sample for selected soil layers (Table 1). Soil samples were then grouped into the following depth intervals: topsoil: 0–10 cm; subsoil: 30–50 cm, except for colluvial profiles of the NC and SC sites where the subsoil

TABLE 1 Descriptions of study sites

Sampling sites	Parent material	Soil type	MAT °C	MAP mm/year	PET mm/year	Main crop	Cultivation history years	Accretion rate mm/year	Slope position	Sampling depth cm
Spain (SP) (42°25′28.14″N, 1°13′36.09″W) (Warm-arid)	Quaternary deposits	Calcisols	13.4	500	1355	Winter wheat	~120	8.33	Non-colluvial	0–10
										30–50
									Colluvial	0–10
										30–50
NW China (NC) (35°3′18.45″N, 109°38′25.34″ E) (Warm-arid)	Loess	Cambisols	13.2	540	1388	Wheat Corn	>1000	4.54	Non-colluvial	0–10
										30–50
									Colluvial	0–10
										30–45
Belgium (BE) (50°45′40.53″N, 4°44′8.91″ E) (Warm-humid)	Calcareous loess	Luvisols	11	805	726	Maize	c. 300–2300 BP	2.90	Non-colluvial	0–10
										30–50
									Colluvial	0–10
										30–50
S China (SC) (24°18′42.16″N, 113°46′7.84″ E) (Tropical)	Granite	Ferralsols	21.5	1649	1341	Cereals	<80	4.97	Non-colluvial	0–10
										30–50
									Colluvial	0–10
										30–45
S Brazil (SB) (28°51′36.9″S, 52°04′59.4″W) (Tropical)	Acidic rhyodacite rocks	Acrisols	24.1	1700	1281	Corn soybean tobacco	~95	2.01	Non- colluvial	0–10
										30–50
									Colluvial	0–10
										30–50

Note: Abbreviations are listed in Table 2. PET data were extracted from Trabucco and Zomer (2018). MAT and MAP data were obtained from https://www.meteoblue.com (last access: August 2020).

TABLE 2 List of abbreviations

Indexes	Abbreviations	Unit
MAT	Mean annual temperature	°C
MAP	Mean annual precipitation	mm/year
PET	Potential evapotranspiration	mm
MAP–PET	Soil effective water	mm
SPR	Soil potential respiration rate	μg C h^{-1} g SOC^{-1}
cPOC	Coarse particulate OC	kg C m^{-2} cm^{-1}_{depth}
mAOC	Microaggregated OC	kg C m^{-2} cm^{-1}_{depth}
s + c	Silt & clay-associated OC	kg C m^{-2} cm^{-1}_{depth}
1:1 N	1:1 Non-expandable clay mineral	%
Fe_d/Fe_t	% of pedogenic Fe oxides to total Fe	-
Fe_p, Al_p, Mn_p	Chelated organo-metal complexes	mg kg^{-1} soil
M_p	Sum of Fe_p, Al_p and Mn_p	mg kg^{-1} soil
$Fe_{o\text{-}p}$, $Al_{o\text{-}p}$, $Mn_{o\text{-}p}$	Poorly crystalline oxides	mg kg^{-1} soil
$Fe_{d\text{-}o}$	Crystalline Fe oxides	mg kg^{-1} soil
$M_{o\text{-}p}$	Sum of $Fe_{o\text{-}p}$, $Al_{o\text{-}p}$, and $Mn_{o\text{-}p}$	mg kg^{-1} soil
1:1 N	1:1 Non-expandable clay mineral	%
2:1 N	2:1 Non-expandable clay mineral	%
2:1E	2:1 Expandable clay mineral	%
CEC	Cation exchange capacity	$cmol_c$ kg^{-1} soil
BS	Base saturation	-
TRB	Total reserve in bases	$cmole_c$ kg^{-1} soil

represented the 30–45 cm soil layer. Samples were collected in 2007, 2014 and 2017 (see Table S1).

2.3 | SOC fractionation, soil respiration and radiocarbon content

Approximately 40 g of 2 mm sieved air-dried soils were fractionated in duplicate to obtain SOC fractions for two slope positions (non-colluvial and colluvial profile) and two depth layers (topsoil and subsoil, see field sampling and Table 1). We used a fractionation scheme based on the conceptual SOC model proposed by Six et al. (1998, 2002) applying a simplified version of its fractionation protocol (detailed in Doetterl, Cornelis, et al., 2015). Total SOC was fractionated into coarse particulate organic carbon (cPOC, >250 μm), microaggregate-associated SOC (mAOC, 250–53 μm) and silt and clay-associated SOC (s + c, <53 μm). All fractions were analysed for total C by dry combustion (CHN628 Series Leco Elemental Determinator, USA). Samples from NC and SP sites contained inorganic C that was measured by the calcimeter method, as described in Sherrod et al. (2002). SOC content was then derived from the total C by subtraction of the measured inorganic C.

To determine the soil-specific potential maximum heterotrophic respiration (SPR), we incubated three replicate samples of 50 g 2-mm sieved bulk soils (same samples as for SOC fractionation and soil chemical properties). A 10-day pre-incubation was carried out in order to avoid CO_2 pulses caused by soil sample preparation (i.e., sieving, drying and rewetting), and then respiration was monitored over 8 weeks keeping moisture (60% of soil water holding capacity) and temperature (20°C) constant to determine SPR. Samples of the gas mixture within incubation jars were taken periodically every three to seven days throughout the experiment. The gas samples were then analysed for CO_2 concentration using a Picarro G2131–I gas analyser (Picarro Inc., Santa Clara, USA). We followed the incubation protocol used by Doetterl, Stevens, et al. (2015).

Radiocarbon content was measured for the bulk soil from five colluvial profiles. Additionally, radiocarbon analysis was conducted for the microaggregated and silt & clay-associated SOC fractions of colluvial profiles from warm-arid (SP site), temperate (BE site) and tropical (SC site) climate regions. We further linked the depth patterns of percent modern carbon (pMC) to weathering degree and soil geochemistry properties by calculating the ratio of subsoil to topsoil for geochemical variables. These analyses can provide insights into how soil accretion affects weathering status and soil mineral matrix and thus the colluvial SOC stability. Radiocarbon content was measured at the Max Planck Institute for Biogeochemistry (Jena, Germany). Soil samples were combusted and reduced to graphite according to Steinhof et al. (2017) prior to analysis by accelerator mass spectrometer (AMS) (MICADAS, Ionplus, Dietikon, Switzerland). Samples from SP site contained inorganic C that was separated by acid hydrolysis. Results were expressed as fraction modern ($F^{14}C$), which was the fraction with respect to the standard isotope ratio including normalisation for $\delta^{13}C$. pMC was calculated from $F^{14}C$ by multiplying 100 (Stuiver & Polach, 1977). All fraction

modern data and associated measurement errors were provided in Table S1.

2.4 | Soil physical–chemical properties

Using bulk soils from non-colluvial and colluvial soil profiles for top- and subsoil layers at each study site, key soil physical–chemical properties were measured. 2-mm sieved soils were used for soil texture and pH_{H2O} measurements. Milled soils were used for analysing cation exchange capacity (CEC), base saturation (BS), elemental composition of the soil solid phase (Fe, Mn, Al, Si, K, Ca, Na, Mg), total reserve in bases (TRB), chelated organo-metal complexes (Fe_p, Al_p and Mn_p), poorly crystalline oxides ($Fe_{o\text{-}p}$, $Al_{o\text{-}p}$ and $Mn_{o\text{-}p}$), crystalline Fe oxides ($Fe_{d\text{-}o}$), and soil clay-sized mineralogy (non–expandable 1:1 layered (1:1 N), non–expandable 2:1 layered (2:1 N) and expandable 2:1 layered (2:1E) minerals). These measurements provide additional support to explain the different mechanisms of SOC stability between non-colluvial and colluvial soils.

The concentration of chelated organo-metal complexes (Fe_p, Al_p and Mn_p) was measured using sodium pyrophosphate following Bascomb (1968). The amount of poorly crystalline oxides plus organically complexed Fe, Al and Mn were measured by extraction with ammonium oxalate–oxalic at pH = 3 following Blakemore et al. (1987); poorly crystalline oxides ($Fe_{o\text{-}p}$, $Al_{o\text{-}p}$ and $Mn_{o\text{-}p}$) were estimated by the difference between oxalate and pyrophosphate extractable ions. The total concentration of pedogenic Fe, Al and Mn oxides were quantified through extraction with Dithonite–Citrate–Bicarbonate (DCB) following Mehra and Jackson (1960); the difference between this measurement and oxalate extractable ions provided an approximation of the crystalline Fe oxides ($Fe_{d\text{-}o}$) (Berhe et al., 2012; Masiello et al., 2004). The molar ratio was calculated according to Oades et al. and Masiello et al. (Masiello et al., 2004; Oades, 1989). If the molar ratio value falls within the range of 2–10, it indicates that chelation of organic acids with Fe^{3+} and Al^{3+} to form organo–metal complexes are the dominant mechanism of C stabilisation in tested samples, otherwise, it suggests that another mechanism may be responsible for SOC chemical stabilisation. Fe_d/Fe_t, representing the proportion of pedogenic iron oxides to total iron, was expected to increase with weathering and thus widely used as a weathering indicator (Arduino et al., 1986). All extracts were analysed for their Fe, Al and Mn content using ICP–AES. Elemental contents (K, Ca, Na, Mg, Si, Al, Fe and Mn) in soils were determined by ICP–AES after alkaline fusion using Li–metaborate + Li–tetraborate at 1000°C, followed by ash dissolution with concentrated HNO_3 (Chao & Sanzolone, 1992). The loss on ignition (LOI) was assessed at 1000°C and the total element contents are expressed in reference to the soil dry weight at 105°C. TRB, a measure of four alkaline and alkaline–earth cations, was expected to decrease as cations are leached during weathering (Herbillon, 1986).

Soil texture was analysed using a laser diffraction particle size analyser (Model LS 13320; Beckman Coulter Inc., Fullerton, USA) after ultrasonic dispersion and removal of organic matter using H_2O_2 (35%) (Beuselinck et al., 1998). Soil pH_{H2O} was determined with a soil/solution ratio of 1:5 (w/v) with demineralized water using a pH–meter (Mettler Toledo MP220, Mettler–Toledo, Switzerland). CEC was determined by quantifying exchangeable NH_4^+ displaced with KCl (10%, pH = 3) after saturating cation exchange sites with 1 M ammonium acetate buffered at pH 7.0 and measured with inductively coupled plasma–atomic emission spectrometry (ICP–AES, Jarrell Ash Iris Advantage) (Chapman, 1969).

The phyllosilicate minerals of clay fractions were determined by X-ray diffraction (XRD, Empyrean Panalytical) after removing Fe oxides by the DCB extraction method. For XRD measurements, specimens were saturated with K^+ or Mg^{2+} solution and mounted as slurries on glass slides. The air-dried Mg saturated specimens were analysed at 25°C and after ethylene glycol solvation overnight. The air-dried K-saturated specimens were X–rayed at 25°C before and after heating at 105, 300 and 550°C for 2 h (Robert & Tessier, 1974). All XRD patterns were recorded by an Empyrean Tube X-ray equipped with a PIXcel3D detector (Malvern Panalytical Ltd, Netherlands) using Cu Kα radiation generated with 40 kV, accelerating potential and 40 mA tube current, from 2 to 30° (2θ). Clay minerals were identified according to a handbook (Moore & Reynolds, 1997). Quantification of clay minerals was performed by Pawley fit with the direct derivation method using the HighScore Plus 4.8 software (Malvern Panalytical Ltd, UK). The direct derivation method is a new method that can quantify multi–component polycrystalline materials with intermediate to high accuracy (Toraya, 2016). The refinement process was carried out following the help file of HighScore Plus 4.8. Key primary minerals that can interfere with the reflection patterns and exist in clay fractions such as quartz, feldspar, calcite and mica were quantified. We then focused on secondary minerals. Note that no distinction was made between primary and secondary chlorite. Finally, we grouped secondary minerals into non–expandable 1:1 layered (1:1 N), non–expandable 2:1 layered (2:1 N) and expandable 2:1 layered (2:1E) minerals.

TABLE 3 Measurements of soil chemical properties

Sites	Slope position	Soil depth	Clay %	Silt	Sand	pH	CEC $cmol^{+}$	TRB kg^{-1}	Molor ratio	Al_p	Fe_p mg kg^{-1} soil	Mn_p	Al_{o-p}	Fe_{o-p}	Mn_{o-p}	Fe_{d-o}	1:1 N %	2:1 N %	2:1E %
SP (Warm arid)	Non-colluvial	top	27.8	67.1	5.0	8.7	7.7	1045	89.8	127	135	30	201	73	34	8166	11.6	40.0	13.1
		sub	31.3	67.1	1.6	8.9	6.6	1058	10.2	76	123	27	67	76	27	7627	6.6	51.8	14.2
	Colluvial	top	24.1	61.1	14.8	8.3	8.7	975	45.7	126	111	52	275	222	38	7245	13.8	34.8	15.0
		sub	29.0	61.9	9.1	8.7	9.8	925	36.4	182	132	46	365	313	63	8428	8.9	39.7	13.9
NC (Warm arid)	Non-colluvial	top	14.0	82.3	3.7	8.3	8.9	606	89.2	103	40	11	531	504	138	6757	7.3	31.2	22.9
		sub	13.6	82.7	3.7	8.5	9.6	590	80.2	96	36	5	642	540	198	6928	9.8	40.9	20.6
	Colluvial	top	17.0	79.4	3.6	8.5	10.9	605	90.6	104	40	5	628	598	169	6749	13.0	21.9	28.1
		sub	13.8	82.8	3.4	8.5	11.1	630	95.2	102	36	4	633	466	162	6809	14.1	31.4	31.2
BE (Temperate)	Non-colluvial	top	10.3	78.1	11.6	7.5	9.9	132	10.6	228	553	146	617	2237	236	3569	18.8	20.4	16.5
		sub	12.2	79.6	8.2	7.7	12.3	137	5.2	230	332	29	905	2429	271	7152	23.1	30.7	6.7
	Colluvial	top	11.2	75.4	13.4	7.5	10.9	126	12.6	167	359	133	473	1381	204	5548	21.0	29.5	16.8
		sub	11.7	75.0	13.4	7.5	10.4	124	6.7	175	226	36	641	1607	297	6294	22.4	17.1	13.0
SC (Sub-tropical)	Non-colluvial	top	10.4	57.8	31.9	5.0	6.5	58	4.6	734	1220	12	255	391	4	15,089	21.1	17.2	26.6
		sub	7.4	58.3	34.3	4.8	8.3	101	2.8	591	623	39	393	415	81	31,634	29.9	15.5	30.8
	Colluvial	top	13.8	51.4	34.8	5.1	4.3	48	5.1	553	1222	8	90	156	0.0	9966	16.6	23.7	34.1
		sub	18.4	55.7	25.9	5.7	5.8	65	5.3	314	296	27	328	389	29	19,067	16.5	24.4	34.6
SB (Sub-tropical)	Non-colluvial	top	15.3	63.7	21.0	6.0	25.3	133	5.3	2270	1260	33	1386	1143	231	10,887	14.2	9.3	25.8
		sub	23.3	65.9	10.9	6.2	16.9	87	4.5	1539	2393	41	1148	2435	292	17,766	32.3	12.9	17.9
	Colluvial	top	22.6	65.7	11.7	5.2	14.5	92	6.4	1477	1562	168	914	3044	470	16,898	22.2	8.6	29.1
		sub	23.6	65.3	11.1	5.2	17.2	91	5.8	1614	1814	163	1176	3503.2	703	16,820	26.7	14.7	17.4

Note: Abbreviations are listed in Table 2.

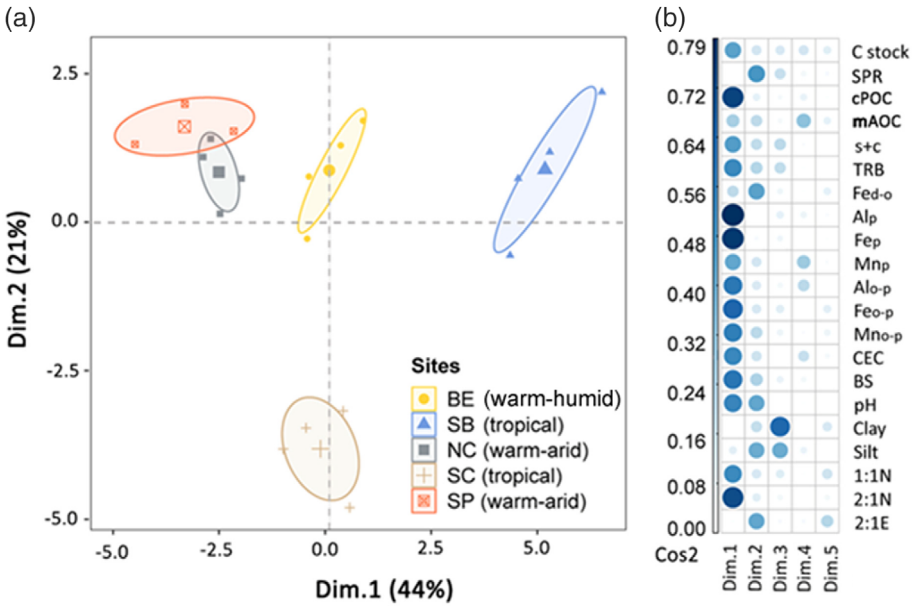

FIGURE 1 Principal components analysis (PCA) showing the differences between the sites. (a) PCA biplot. The percentage of variance explained by each PC is shown in parentheses. (b) Visualisation of quality of representation of variables in top five dimensions. Cos2 is the quality of representation of the variables in the principal component maps. Abbreviations are listed in Table 2

TABLE 4 SOC stock, potential soil respiration (SPR) and SOC fractions

Sites	Slope position	Soil depth	SOC stock $g\ C\ m^{-2}\ cm^{-1}_{depth}$	SPR $\mu g\ C\ h^{-1}\ g\ SOC^{-1}$	cPOC Percentage of total SOC (%)	mAOC	s + c
SP	Non-colluvial	top	133	27.5 ± 4.6 b	0.7 ± 0.0 b	55.5 ± 8.3 a	43.7 ± 8.3 a
		sub	42	17.6 ± 0.6 c	ns	22.2 ± 11.0 a	77.8 ± 11.1 a
	Colluvial	top	147	56.1 ± 2.7 a	7.0 ± 1.9 a	36.6 ± 2.0 a	56.4 ± 6.9 a
		sub	231	11.1 ± 0.5 c	1.1 ± 0.1 b	41.2 ± 11.3 a	57.7 ± 11.4 a
NC	Non-colluvial	top	104	30.9 ± 0.5 a	7.7 ± 3.5 ab	34.9 ± 15.8 a	57.3 ± 19.4 a
		sub	57	23.9 ± 2.4 b	20.0 ± 5.7 a	30.1 ± 4.8 a	49.9 ± 0.8 a
	Colluvial	top	79	24.4 ± 2.1 b	4.3 ± 1.3 b	30.5 ± 3.0 a	65.2 ± 4.3 a
		sub	48	17.3 ± 1.0 c	4.9 ± 3.2 b	36.8 ± 1.0 a	58.3 ± 7.2 a
BE	Non-colluvial	top	175	28.5 ± 2.5 a	5.7 ± 0.8 a	52.5 ± 1.4 a	41.8 ± 2.2 b
		sub	60	24.2 ± 3.5 ab	1.4 ± 0.1 b	45.5 ± 3.0 ab	53.1 ± 2.9 a
	Colluvial	top	181	27.5 ± 1.1 a	4.3 ± 0.7 a	42.5 ± 2.0 b	53.2 ± 2.7 a
		sub	54	19.9 ± 3.7 b	1.0 ± 0.3 b	42.0 ± 3.0 b	57.1 ± 3.2 a
SC	Non-colluvial	top	135	15.6 ± 0.5 a	6.8 ± 0.0 a	41.1 ± 2.0 ab	52.1 ± 1.9 b
		sub	47	12.5 ± 0.5 b	4.6 ± 1.1 ab	42.4 ± 0.3 a	53.1 ± 0.8 b
	Colluvial	top	116	15.7 ± 1.6 a	4.7 ± 1.2 ab	42.4 ± 0.1 a	52.9 ± 1.7 b
		sub	54	8.4 ± 0.9 c	2.2 ± 0.3 b	37.9 ± 0.8 b	59.9 ± 1.1 a
SB	Non-colluvial	top	228	17.6 ± 2.5 b	20.3 ± 0.9 a	37.3 ± 1.4 a	42.4 ± 0.4 a
		sub	156	10.6 ± 0.7 c	15.4 ± 0.8 b	34.4 ± 0.4 a	50.2 ± 1.2 a
	Colluvial	top	256	26.6 ± 2.5 a	10.9 ± 0.0 c	36.1 ± 2.4 a	53.0 ± 2.4 a
		sub	202	25.3 ± 2.0 a	19.9 ± 0.6 a	25.4 ± 7.5 a	54.7 ± 8.0 a

Note: Different lowercase letters indicate the significant differences in SPR or SOC fractions between the depth layers or non-colluvial/colluvial soil profiles at $p < 0.1$ level. Data are expressed as mean ± standard deviations.
Abbreviation: cPOC, coarse particulate SOC; mAOC, microaggregates-associated SOC; ns, not enough material left for CN analysis; s + c, silt & clay SOC.

2.5 | Statistical analysis

Statistical analysis was performed using R 4.2.0 (https://www.R-project.org). Principal Component Analysis (PCA) combined with PERMANOVA was used to examine how SOC variables and geochemical properties differ between sampling sites. To assess the influencing factors on soil potential respiration (SPR), linear mixed-effects

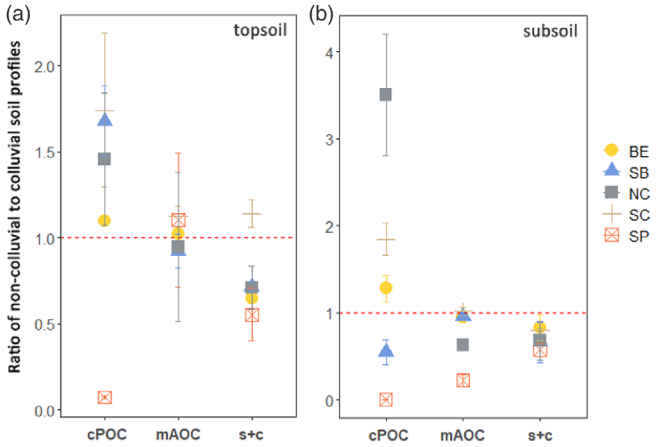

FIGURE 2 SOC fraction distribution as a function of slope positions for (a) topsoil and (b) subsoil layers. Data points are displayed as the ratio values of non-colluvial to colluvial profile; for example, ratio value <1 means the colluvial profile has a higher content of SOC fractions than non-colluvial profile. SOC fractions used to calculate the ratio values are expressed as the C density (kg C m^{-2} cm^{-1}_{depth}). The error bars represent the standard deviation. cPOC, coarse particulate SOC; mAOC, microaggregates-associated SOC; s + c, silt & clay SOC.

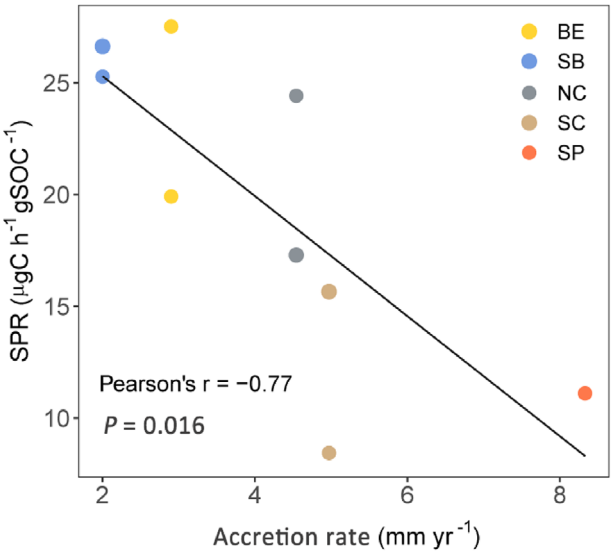

FIGURE 3 Relationship between accretion rate and potential soil respiration (SPR). Datapoints include two depth layers from five colluvial soil profiles

models were fitted, including the factors of climate, weathering, cultivation history and accretion rates as fixed effects. For each fixed effect, a linear mixed-effect model was fitted while controlling for soil depth via a random intercept. The marginal R-square (R^2_m) and conditional R-square (R^2_c) were estimated using the "sjstats" package (Lüdecke, 2019). All linear mixed-effects models were fitted using maximum likelihood methods via the lmerTest package (Kuznetsova et al., 2017). The interaction effects between SPR, climate, weathering, cultivation history and accretion rates were further evaluated using zero-order correlation and partial correlation analysis. Partial correlation analysis is a widely applied statistical tool to isolate the relationship between two variables from the confounding effects of other correlated variables (Jukić & Denić-Jukić, 2015). Partial correlation analysis measures the strength of the linear relationship between two variables (e.g., SPR and Fe_d/Fe_t) depending on the linear effect of other (control) variables (e.g., MAT) (e.g., Jukić & Denić-Jukić, 2015). To avoid overinterpretation caused by the limited sample size ($N = 10$ per slope position), we focus on the partial control that significantly shifted the zero-order correlations at $p < 0.05$ level (Figure 4). Shapiro–Wilk tests were performed to check data normality. Pearson's correlation was used when variables were normally distributed, otherwise, Spearman's correlation was chosen. Differences in means of specific potential respiration (SPR) and SOC fractions between the geomorphic position and depth layer classes were tested by ANOVA using R package "agricolae". To compare the means of multiple groups, post hoc test was applied using Bonferroni correction. During the incubation, lots of seeds in SP colluvial topsoil began to germinate, and the observed SPR of this sample was extremely higher compared to other samples (Table 4). Although we regularly removed the new buds, this most likely affected the results. We, therefore, performed a Bonferroni outlier analysis on the SPR data and confirmed that the SP colluvial topsoil observation was a significant outlier ($p < 0.05$) and therefore excluded it from the regression and correlation analysis.

3 | RESULTS

3.1 | Description of soil properties

Soils were classified as silt loam (NC, BE, SC and SB) and silt clay loam (SP) according to the USDA texture classification system. In general, clay-sized mineralogy of semi-arid and humid regions was dominated by 2:1 non-expandable minerals (e.g., illite). While within the subtropical regions, clay mineralogy of SC site was dominated by 2:1 expandable minerals (smectite), and SB site was dominated by 1:1 non-expandable (kaolinite) and 2:1 expandable minerals (smectite). From warm-arid to subtropical climate regions (Table 3), soil pH and molar ratio values decreased from 8.3–8.9 to 4.8–6.2 and 10.2–95.2 to 2.8–6.4, respectively. While the concentration of Al_p and Fe_p increased from 76–182 mg kg^{-1} to 314–2270 mg kg^{-1} and 36–135 mg kg^{-1} to 296–2393 mg kg^{-1} soil, respectively. In addition, warm-arid

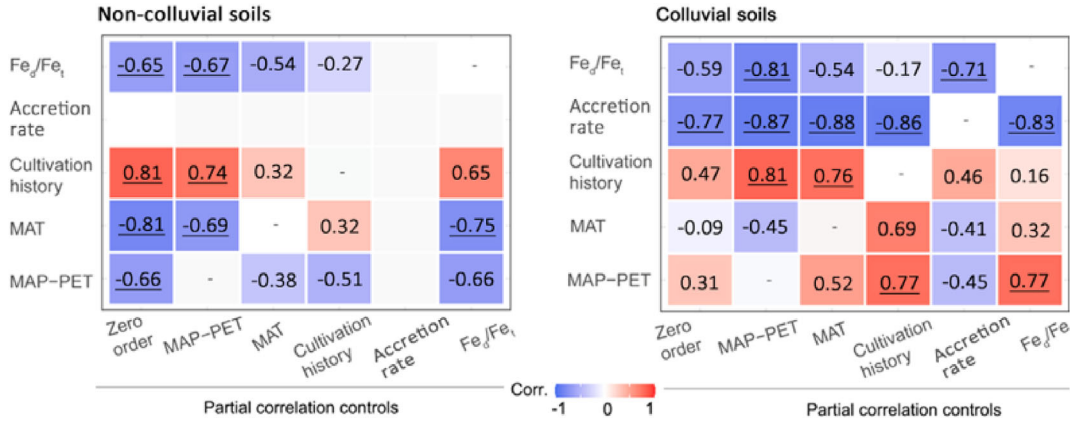

FIGURE 4 Zero-order and partial correlations between potential soil respiration rate (SPR) and controlling factors. Samples include two depth layers from five soil profiles. Difference between zero–order and partial correlations indicate the level of dependency of the correlation between a given predictor and the SOC response (see method). Colours and numbers indicate the strength (the intensity of the colour) and sign (blue and red colours indicate negative and positive correlations, respectively) of correlation. Grey squares mean no values. Underlined numbers indicate $p < 0.05$

TABLE 5 Linear mixed-effect model estimates for potential soil respiration rate (SPR)

Response		Effect	Estimate	SE	*p* value	R^2_m	R^2_c
SPR	Non-colluvial profile	MAT	−1.066	0.156	0.000	0.58	0.90
		MAP-PET	−0.0073	0.003	0.035	0.32	0.57
		Cultivation history	4.255	1.715	0.042	0.31	0.55
		Fe_d/Fe_t	−25.396	9.829	0.036	0.35	0.53
	Colluvial profile	MAT	−0.035	0.427	0.937	0.00	0.19
		MAP-PET	0.002	0.004	0.700	0.02	0.17
		Cultivation history	2.511	2.222	0.308	0.12	0.28
		accretion rate	−2.440	0.721	0.019	0.48	0.68
		Fe_d/Fe_t	−22.185	10.495	0.085	0.28	0.52

Note: Fixed effects include climate (MAT, MAP-PET), cultivation history, weathering status (Fe_d/Fe_t) and accretion rate. For each fixed effect, a linear mixed-effect model was fitted while controlling for soil depth via a random intercept. The estimated *p* values, standard error (SE), marginal R-square (R^2_m) and conditional R-square (R^2_c) are given.

regions had higher TRB but lower $Fe_{d\text{-}o}$ concentration than subtropical regions. No consistent trends in Mn oxides (Mn_p, $Mn_{o\text{-}p}$), CEC and clay-sized minerals (1:1 N, 2:1 N, 2:1E) along the climate gradient could be found. The accretion rates followed the order: SP > SC > NC > BE > SB (Table 1). In general, the differences between sites were much larger than those between the non-colluvial/colluvial profiles for all measured soil properties (Table 3).

The PCA combining with PERMANOVA analysis showed that samples from the semiarid regions (SC, NC sites) were similar but were distinct from samples from other climate zones (Figure 1a). The reactive mineral phases ($Fe_{o\text{-}p}$, $Al_{o\text{-}p}$, $Mn_{o\text{-}p}$, Fe_p, Al_p), soil fertility (CEC, BS, pH, TRB), non-expendable clay minerals (1:1 N, 2:1 N) and cPOC-associated SOC fraction contributed most to

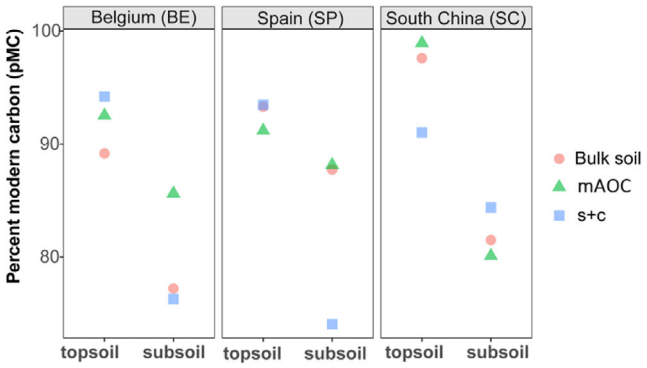

FIGURE 5 Percent modern carbon (pMC) of bulk soil and SOC fractions for colluvial soil profiles. mAOC, microaggregated SOC; s + c, silt & clay-associated SOC.

Dimension 1 (explaining 44% of the observed variance). Dimension 2, which explained 21% of the variance, was largely driven by soil respiration (SPR), expandable clay minerals (2:1E) and crystalline Fe oxides ($Fe_{d\text{-}o}$) (Figure 1b).

3.2 | SOC stock, SOC fractions and soil potential respiration

A broad range of SOC storage (42–256 g $C\ m^{-2}\ cm^{-1}_{depth}$) was observed across sampling sites, with the highest value in subtropical regions (Table 4). For subsoil layers, higher SOC storage was found in colluvial soils of SP, SC SB sites than non-colluvial soils. While in NC and BE sites slightly lower SOC storage was observed in colluvial subsoils than in non-colluvial subsoils. Significant effects of soil depth and geomorphic position on SPR were observed in the incubation experiments. The topsoil respired at a higher rate than subsoil soils per unit C (g), no matter of the slope position. Except for one of subtropical site (SB site), SPR of colluvial subsoil was generally lower than non-colluvial subsoil although the statistical difference ($p < 0.1$) was only observed for NC and SC sites. At all sites and soil depths (Table 4), SOC fractions were dominated by s + c-associated SOC, contributing 41.8 ± 2.2 to 77.8 ± 11.1% of total SOC, and mAOC-associated SOC, contributing 22.2 ± 11.0 to 55.5 ± 8.3% of total SOC. cPOC associated-SOC contributed 1.0 ± 0.3 to 20.3 ± 0.9% of total SOC. Significant differences ($p < 0.1$) in cPOC-associated SOC between depth layers were observed (except for SC site), while the majority of soil profiles did not show statistical differences between depth layers for mAOC (8 out of 10 layer) and s + c-associated SOC (8 out of 10 layers). We observed a clear tendency that the geomorphic position strongly influenced the distribution of s + c-associated SOC (Figure 2): for s + c of subsoil (Figure 2b), ratio values of non-colluvial profile to colluvial profile were consistently lower than 1, meaning more silt and clay-associated SOC in colluvial subsoil than non-colluvial subsoil. For topsoil (Figure 2a), a similar trend was also observed, except for SC site. In contrast, cPOC and mAOC were highly site–specific and no consistent trends could be found.

3.3 | Relationships between SPR and controlling factors

Simple correlation (zero-order) showed that for non-colluvial soils both climate factors (MAT, [MAP-PET]), cultivation history and weathering degree (Fe_d/Fe_t) were significantly correlated with SPR, while for colluvial soils, SPR was significantly correlated to the accretion rate ($p < 0.05$, Figures 3 and 4). Linear mixed-effect models with soil depth as random effect confirmed that for non-colluvial soils, climate factors (MAT, [MAP-PET]) and Fe_d/Fe_t had a negative effect on SPR, while cultivation history had a positive effect on SPR. For colluvial soils, only accretion rate was a significant variable explaining SPR ($p < 0.05$, $R^2_m = 0.48$) (Table 5). Partial correlation analyses (Figure 4) further showed that the significant correlation between accretion rate and SPR for colluvial soils remained constant when controlling for MAT, (MAP-PET), Fe_d/Fe_t or cultivation history. This result suggests that the accretion rate is the most important independent control on colluvial SOC stability. Furthermore, we found that independent of slope position, controlling for cultivation history significantly shifted the correlations between SPR and climate or Fe_d/Fe_t. In addition, for non-colluvial soils, controlling for cultivation history significantly decreased the zero-order correlation between Fe_d/Fe_t and SPR (r decreased from −0.65 to

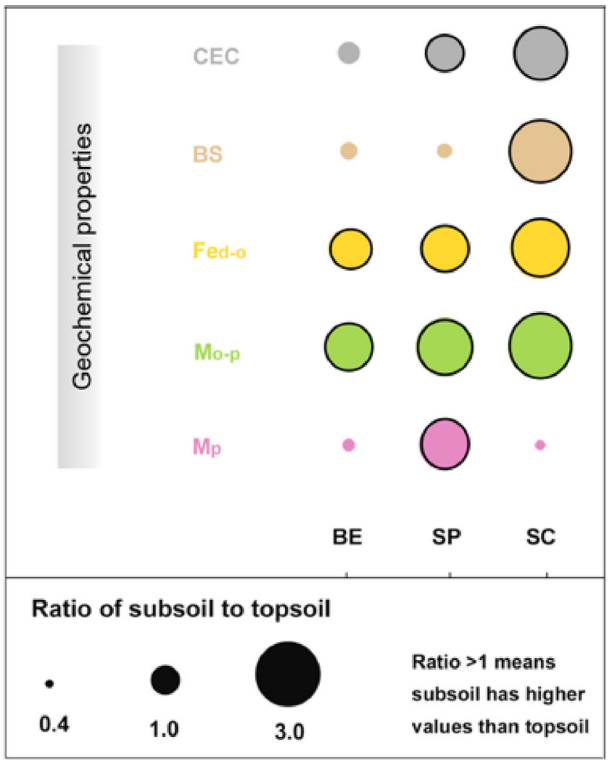

FIGURE 6 Ratio of colluvial subsoil to topsoil for key geochemical properties. Size of circle represents the ratio. Circles with a black outer ring mean the ratio >1.0 and therefore the subsoil has higher values than topsoil. BS, base saturation; CEC, cation exchangeable capacity; $Fe_{d\text{-}o}$, crystalline Fe oxides; $M_{o\text{-}p}$, sum of poorly crystalline Fe, Al and Mn oxides; M_p, sum of chelated organo-metal complexes Fe, Al and Mn

−0.27). While for colluvial soils, controlling for (MAT-PET), cultivation history or accretion rate significantly altered the zero-order correlation between Fe_d/Fe_t and SPR (Figure 4, $p < 0.05$). These results suggest that for non-colluvial soils, the relationship between Fe_d/Fe_t and SPR depends on cultivation history, while for colluvial soils, both effective moisture (MAT-PET), cultivation history and accretion rate are important.

3.4 | Radiocarbon content in colluvial soil profiles

The difference in pMC between topsoil and subsoil was largest for the s + c-associated SOC fraction at the BE and SP sites, while the largest difference in pMC at the SC site was found for the mAOC fraction (Figure 5). Further, the difference in weathering degree (i.e., TRB, Fe_d/Fe_t, K/I) between non-colluvial and colluvial soils was much larger at the SC site than the BE and SP sites (Table S2). Such weathering patterns between sites ultimately reflected the underlying geochemistry: (1) the colluvial subsoil at the SC site had much higher CEC and BS than the topsoil, while the inverse tendency was observed at the BE and SP sites; (2) at the SP site, subsoil had considerably higher content of organo-metal complexes (M_p = sum of Fe_p, Al_p and Mn_p) than the topsoil, and the pMC difference between soil depth layers was largest for s + c-associated SOC fraction (Figure 6).

4 | DISCUSSION

The linear mixed-effect models and correlation analysis suggest that the rate of accretion is the most important control on colluvial SOC stability (Figure 3 and Table 5). The partial correlation analysis further reveals that the importance of accretion rate in influencing colluvial SOC dynamic is independent of climate and geochemical context, as the significant correlation between accretion rate and SPR for colluvial soils is not influenced by controlling for other factors (Figure 4). Our results are corroborated by model simulation output on the role of soil deposition for SOC stability in colluvial soils for a fine-textured soil in a temperate region (Wang et al., 2015). This study reported that the accretion rate controls the time that buried soil spends at a given soil depth, thereby controlling the temporal evolution of C input and decomposition rate during the burial process. Importantly, higher accretion rates seem to increase the equilibrium SOC content of the colluvial soil profile, irrespective of climatic or geochemical context. In addition, we found that accretion rate is negatively correlated with SPR (Figure 3), indicating that the colluvial SOC with higher rate of accretion is more stable. This is in line with the notion that the decomposition rate of colluvial SOC can be reduced by a combination of biochemical (recalcitrance of OC constituents), physical (e.g., protected with burial, aggregation) and chemical (e.g., organo-mineral associations) processes (Berhe et al., 2007; Mariappan et al., 2022). On the one hand, the deposited labile SOC in colluvial settings can be rapidly mineralized in-situ (Van Oost et al., 2012; Wang, Van Oost, et al., 2014), resulting in more recalcitrant, remaining SOC fraction becoming eventually buried. On the other hand, higher accretion rates are associated with more intensively weathered topsoil together with finer particles and reactive minerals (e.g., smectite) within colluvial settings (Doetterl, Cornelis, et al., 2015). As a result, more s + c-associated SOC was accumulated in colluvial settings than non-colluvial soils as shown in Figure 2. Since colluvial subsoil is buried under the previous topsoil, accumulation of highly weathered topsoil and s +- c-associated SOC (Table 3, Figure 2) changes the weathering status and mineral matrix of colluvial soil settings, especially in subsoils, compared to their non-colluvial profile counterparts. The interaction effect of weathering on SOC stabilisation is supported by the outcome of our partial correlation analysis: controlling for accretion rate significantly increased the correlation between Fe_d/Fe_t and SPR (Figure 4, $p < 0.05$). The weathering–dependent SOC stabilisation has been ascribed to the facilitation of complexation and adsorption of SOC with minerals, enhancing mineral (organo–mineral associations) and/or physical SOC protection mechanisms via soil aggregation (Denef & Six, 2005; Doetterl et al., 2018; Duiker et al., 2003; Dümig et al., 2011).

The pronounced weathering–dependent SOC stabilisation mechanism in colluvial soils is further supported by the radiocarbon content (pMC) of SOC fractions in selected colluvial profiles (Figures 5 and 6). We found that the difference in pMC between topsoil and subsoil is largest for the s + c SOC fraction at the BE and SP sites, while the largest radiocarbon difference at the SC site was found for the mAOC fraction (Figure 5). These results suggest that at the BE and SP sites, SOC of colluvial subsoil is predominantly protected by organo-mineral associations (s + c SOC fraction), while at the SC site microaggregation protection (mAOC fraction) plays a major role in SOC stabilisation. Radiocarbon data coupled with geochemical measurements further shows that the less weathered colluvial subsoil (SC site as an example, Table 3) is concomitant with higher CEC, BS

and poorly crystalline oxides than topsoil (Figure 6), leading to microaggregation (e.g., mAOC fraction, SC site) as the leading SOC protection mechanism for colluvial subsoils (Figure 5). In comparison, physico-chemical protection (e.g., s + c SOC fraction) predominately controls the colluvial subsoil SOC stabilisation at the SP and BE sites (Figure 5). These subsoils are characterised by a slightly higher or comparable weathering status and correspondingly lower CEC and BS, along with higher organic metals (especially in SP site) compared to the topsoil (Figure 6 and Table 3). Although the sample size is small (only colluvial profiles from three sites were analysed for ^{14}C of total SOC and two SOC fractions), radiocarbon measurements provide additional evidence for the important role of mineral weathering in controlling colluvial SOC stabilisation.

The duration of cultivation period has been identified as a key factor controlling SOC dynamics (Guo & Gifford, 2002). Long-term cultivation reduces SOC storage (Wang et al., 2019; Zhao et al., 2018), but the losses vary depending on the climate conditions that influence the plant and soil processes driving SOC dynamics (Miller et al., 2004; Ogle et al., 2005). Our results suggest that such interactive effect of cultivation and climate on SOC stability is both evident in non-colluvial and colluvial soils: partial correlation showed that regardless of slope position, controlling for cultivation history significantly shifted the zero-order correlations between SPR and climate (Figure 4). In addition, we found that controlling for cultivation history also significantly changed the zero-order correlations between SPR and mineral weathering (Fe_d/Fe_t), regardless of slope position (Figure 4). These results suggest that the cultivation duration could also indirectly affect SOC stability through its interaction with mineral weathering, and this is evident in both non-colluvial and colluvial soils. This finding is consistent with Huang et al. (2021) that reported intensive cultivation practices (tillage mixing and fertilisation) having significant effects on the weathering of minerals, for example, transformation among expandable vermiculite, smectite and non-expandable illite and shift in iron species and crystallinity.

In non-colluvial soils, we found that climate factors are significantly related to SPR ($p < 0.05$). In contrast, this relationship is insignificant for colluvial soil ($r = -0.09 \sim 0.31$). However, controlling for Fe_d/Fe_t by partial correlation significantly increased the correlation between climate (MAP-PET) and SPR ($r = 0.31 \sim 0.77$) (Figure 4). This suggests that the more pronounced role of weathering-driven stabilisation in colluvial SOC (detailed above) may obscure the direct influence of climate on colluvial SOC dynamics. This may be because, compared to non-colluvial soils, the soil physical properties (e.g., soil volumetric water content, compaction and pore space [i.e., acting as barriers for gas diffusion]) play a more important role than soil temperature in colluvial SOC dynamics (Wiaux et al., 2014, 2015). In addition, colluvial soil is generally located at a valley or concave slope position, potentially receiving more water from surface runoff or ground water. On one hand, higher water availability in colluvial soils can support larger biomass and deeper mineral weathering degree, thus increasing C input and enhancing the mineral weathering-dependent SOC stabilisation (Masiello et al., 2004). This is also revealed by the higher total reserve in bases (TRB, as a weathering indicator) in colluvial topsoil than non-colluvial topsoil (Table 3). On the other hand, higher water availability in colluvial soils creates an anaerobic environment, which is less favourable for decomposers to decompose OC (Wang, Van Oost, et al., 2014; Wiaux et al., 2014). Combining our results with those of the literature, we suggest that the different hydrological regimes and physical properties of colluvial soils (Wiaux et al., 2014, 2015) together with geomorphic processes, have the potential to enhance the importance of weathering-driven SOC stabilisation while may obscure the direct influence of climate on colluvial SOC dynamics. However, due to the lack of soil hydrological and physical measurements, and the relatively small sample size in current study, further investigations are needed to confirm the above mechanisms.

5 | CONCLUSIONS

Our analysis suggests that the dominant controls on SOC stability for colluvial soils are different from those for non-colluvial soils. The rate of soil accretion was identified as the most important independent control of colluvial SOC stability. The rate of accretion also indirectly affected SOC stability by interacting with the weathering degree of colluvial soils; deposition changes the average weathering status and mineral matrix of colluvial (sub)soil settings which affect mineral–dependent SOC physical and physico-chemical protection mechanisms. Our results are in line with the classical notion that climate factors are key to explaining SOC stability in non-colluvial soils. However, we found no direct correlation between climate and SOC variables for a broad range of colluvial soils. This is likely due to the different hydrological regimes and physical properties of colluvial soils, that together with physical soil redistribution processes, have the potential to enhance the weathering-driven SOC stabilisation in colluvial soils. This may therefore obscure the direct influence of climate on colluvial SOC dynamics. This study suggests the need to consider both the direct effect of accretion rate as well

as its indirect effects (via influence on weathering status and soil mineral matrix) on colluvial SOC stabilisation when evaluating the fate of eroded SOC. Due to the relatively small but diverse sample size, this conclusion should be regarded as a working hypothesis from which to design future targeted investigations.

AUTHOR CONTRIBUTIONS

Pengzhi Zhao: Conceptualization (lead); investigation (lead); methodology (lead); visualization (lead); writing – original draft (lead); writing – review and editing (lead). **Sebastian Doetterl:** Conceptualization (equal); methodology (equal); resources (equal); supervision (equal); writing – review and editing (equal). **Zhengang Wang:** Conceptualization (equal); resources (equal); writing – review and editing (equal). **Alison M. Hoyt:** Resources (equal); validation (equal); writing – review and editing (equal). **Enheng Wang:** Resources (equal); writing – review and editing (equal). **Hanqing Yu:** Resources (equal); writing – review and editing (equal). **Laura Quijano:** Investigation (equal); writing – review and editing (equal). **Daniel J. Fallu:** Investigation (equal); writing – review and editing (equal). **Antony G. Brown:** Project administration (equal); resources (equal); writing – review and editing (equal). **Johan Six:** Conceptualization (equal); resources (equal); writing – review and editing (equal). **Kristof Van Oost:** Conceptualization (equal); funding acquisition (equal); project administration (equal); resources (equal); supervision (equal); validation (equal); writing – review and editing (equal).

ACKNOWLEDGEMENTS

This research was financially supported by the FNRS, Belgium and European Research Council, H2020 (grant no. TerrACE [787790]). Pengzhi Zhao wishes to thank the joint grant from China Scholarship Council and UCLouvain (No. 201706600009), and the FNRS Mobility grant to support a short stay at Sustainable Agroecosystems Group in ETH, Zurich. Kristof Van Oost is a Research Director of FNRS Belgium. Alison M. Hoyt was funded by the European Research Council (Horizon 2020 Research and Innovation Programme, grant agreement 695101). The authors would like to thank Marco Bravin, Anne Iserentant, Britta Jahn-Humphrey, Mario Reichenbach, Anton Jesche, Manuel Rost and Joseph Okello for their assistance with the soil geochemical and mineralogical analysis. Pengzhi Zhao wishes to thank Prof. Asmeret Asefaw Berhe and Prof. Bruno Delvaux for their patient help with the early stage of data analysis.

CONFLICT OF INTEREST

The authors declare that there is no conflict of interest.

DATA AVAILABILITY STATEMENT

The data that support the findings of this study are available from the corresponding author upon reasonable request.

ORCID

Pengzhi Zhao https://orcid.org/0000-0001-6675-7338
Sebastian Doetterl https://orcid.org/0000-0002-0986-891X

REFERENCES

Arduino, E., Barberis, E., Ajmone Marsan, F., Zanini, E., & Franchini, M. (1986). Iron oxides and clay minerals within profiles as indicators of soil age in northern Italy. *Geoderma*, *37*(1), 45–55. https://doi.org/10.1016/0016-7061(86)90042-X

Bascomb, C. L. (1968). Distribution of pyrophosphate-extractable iron and organic carbon in soils of various groups. *Journal of Soil Science*, *19*(2), 251–268. https://doi.org/10.1111/j.1365-2389.1968.tb01538.x

Berhe, A. A., Harden, J. W., Torn, M. S., Kleber, M., Burton, S. D., & Harte, J. (2012). Persistence of soil organic matter in eroding versus depositional landform positions. *Journal of Geophysical Research – Biogeosciences*, *117*(2), 1–16. https://doi.org/10.1029/2011JG001790

Berhe, A. A., Harte, J., Harden, J. W., & Torn, M. S. (2007). The significance of the erosion-induced terrestrial carbon sink. *Bioscience*, *57*(4), 337–346. https://doi.org/10.1641/B570408

Beuselinck, L., Govers, G., Poesen, J., Degraer, G., & Froyen, L. (1998). Grain-size analysis by laser diffractometry: Comparison with the sieve-pipette method. *Catena*, *32*(3–4), 193–208. https://doi.org/10.1016/S0341-8162(98)00051-4

Blakemore, L. C., Searle, P. L., & Daly, B. K. (1987). *Methods for chemical analysis of soils* (Second Rev ed.). New Zealand Soil Bureau Scientific Report 10 A.

Blume, H.-P., Brümmer, G. W., Horn, R., Kandeler, E., Kögel-Knabner, I., Kretzschmar, R., et al. (2016). *Scheffer/Schachtschabel soil science* (Vol. 16). Springer. https://doi.org/10.1007/978-3-642-30942-7

Carvalhais, N., Forkel, M., Khomik, M., Bellarby, J., Jung, M., Migliavacca, M., et al. (2014). Global covariation of carbon turnover times with climate in terrestrial ecosystems. *Nature*, *514*(7521), 213–217. https://doi.org/10.1038/nature137310

Chao, T. T., & Sanzolone, R. F. (1992). Decomposition techniques. *Journal of Geochemical Exploration*, *44*(1–3), 65–106.

Chapman, H. D. (1969). Cation exchange capacity. In *Methods of Soil Analysis* (Vol. 1, pp. 891–900). American Society of Agronomy.

Denef, K., & Six, J. (2005). Clay mineralogy determines the importance of biological versus abiotic processes for macroaggregate formation and stabilization. *European Journal of Soil Science*, *56*(4), 469–479. https://doi.org/10.1111/j.1365-2389.2004.00682.x

Doetterl, S., Berhe, A. A., Arnold, C., Bodé, S., Fiener, P., Finke, P., et al. (2018). Links among warming, carbon and microbial dynamics mediated by soil mineral weathering.

Nature Geoscience, *11*(8), 589–593. https://doi.org/10.1038/s41561-018-0168-7

Doetterl, S., Cornelis, J. T., Six, J., Bodé, S., Opfergelt, S., Boeckx, P., & Van Oost, K. (2015). Soil redistribution and weathering controlling the fate of geochemical and physical carbon stabilization mechanisms in soils of an eroding landscape. *Biogeosciences*, *12*(5), 1357–1371. https://doi.org/10.5194/bg-12-1357-2015

Doetterl, S., Stevens, A., Six, J., Merckx, R., Van Oost, K., Casanova Pinto, M., et al. (2015). Soil carbon storage controlled by interactions between geochemistry and climate. *Nature Geoscience*, *8*(10), 780–783. https://doi.org/10.1038/ngeo2516

Duiker, S. W., Rhoton, F. E., Torrent, J., Smeck, N. E., & Lal, R. (2003). Iron (hydr)oxide crystallinity effects on soil aggregation. *Soil Science Society of America Journal*, *67*(2), 606–611. https://doi.org/10.2136/sssaj2003.6060

Dümig, A., Smittenberg, R., & Kögel-Knabner, I. (2011). Concurrent evolution of organic and mineral components during initial soil development after retreat of the Damma glacier, Switzerland. *Geoderma*, *163*(12), 83–94. https://doi.org/10.1016/j.geoderma.2011.04.006

Feng, W., Liang, J., Hale, L. E., Jung, C. G., Chen, J., Zhou, J., Xu, M., Yuan, M., Wu, L., Bracho, R., Pegoraro, E., Schuur, E. A. G., & Luo, Y. (2017). Enhanced decomposition of stable soil organic carbon and microbial catabolic potentials by long-term field warming. *Global Change Biology*, *23*(11), 4765–4776. https://doi.org/10.1111/gcb.13755

Guo, L. B., & Gifford, R. M. (2002). Soil carbon stocks and land use change: A meta analysis. *Global Change Biology*, *8*(4), 345–360. https://doi.org/10.1046/j.1354-1013.2002.00486.x

Herbillon, A. J. (1986). Chemical estimation of weatherable minerals present in the diagnostic horizons of low activity clay soils. In F. H. Beinroth, M. N. Camargo, & Eswaran (Eds.), *Proceedings of the 8th International Clay Classification Workshop: Classification, Characterization and Utilization of Oxisols (part 1)* (pp. 39–48).

Huang, C., Meng, S., Tan, W., Wen, S., Li, D., Wang, B., & Koopal, L. K. (2021). Regional differences in mineral weathering characteristics of zonal soils under intensive agriculture. *Applied Clay Science*, *215*, 106336. https://doi.org/10.1016/j.clay.2021.106336

Jukić, D., & Denić-Jukić, V. (2015). Investigating relationships between rainfall and karst-spring discharge by higher-order partial correlation functions. *Journal of Hydrology*, *530*, 24–36. https://doi.org/10.1016/j.jhydrol.2015.09.045

Kramer, M. G., & Chadwick, O. A. (2018). Climate-driven thresholds in reactive mineral retention of soil carbon at the global scale. *Nature Climate Change*, *8*(12), 1104–1108. https://doi.org/10.1038/s41558-018-0341-4

Kuznetsova, A., Brockhoff, P. B., & Christensen, R. H. (2017). lmerTest package: Tests in linear mixed effects models. *Journal of Statistical Software*, *82*, 1–26. https://doi.org/10.18637/jss.v082.i13

Li, Y., Quine, T. A., Yu, H. Q., Govers, G., Six, J., Gong, D. Z., et al. (2015). Sustained high magnitude erosional forcing generates an organic carbon sink: Test and implications in the loess plateau, China. *Earth and Planetary Science Letters*, *411*, 281–289. https://doi.org/10.1016/j.epsl.2014.11.036

Liu, Z., Colin, C., Huang, W., Phon Le, K., Tong, S., Chen, Z., & Trentesaux, A. (2007). Climatic and tectonic controls on weathering in South China and Indochina peninsula: Clay mineralogical and geochemical investigations from the pearl, red, and Mekong drainage basins. *Geochemistry, Geophysics, Geosystems*, *4*(3), 260–266. https://doi.org/10.1029/2006GC001490

Lizaga, I., Quijano, L., Gaspar, L., & Navas, A. (2018). Estimating soil redistribution patterns with ^{137}Cs measurements in a Mediterranean mountain catchment affected by land abandonment. *Land Degradation and Development*, *29*, 105–117. https://doi.org/10.1002/ldr.2843

Lüdecke, D. (2019). *Package 'sjstats'. Statistical functions for Regression Models, Version 0.17* (p. 3). https://mran.revolutionanalytics.com/snapshot/2019-02-07/web/packages/sjstats/sjstats.pdf

Luo, Z., Feng, W., Luo, Y., Baldock, J., & Wang, E. (2017). Soil organic carbon dynamics jointly controlled by climate, carbon inputs, soil properties and soil carbon fractions. *Global Change Biology*, *23*(10), 4430–4439. https://doi.org/10.1111/gcb.13767

Mariappan, S., Hartley, I. P., Cressey, E. L., Dungait, J. A., & Quine, T. A. (2022). Soil burial reduces decomposition and offsets erosion-induced soil carbon losses in the Indian Himalaya. *Global Change Biology*, *28*(4), 1643–1658. https://doi.org/10.1111/gcb.15987

Masiello, C. A., Chadwick, O. A., Southon, J., Torn, M. S., & Harden, J. W. (2004). Weathering controls on mechanisms of carbon storage in grassland soils. *Global Biogeochemical Cycles*, *18*(4), 1–9. https://doi.org/10.1029/2004GB002219

Mehra, O. P., & Jackson, M. L. (1960). Iron oxide removal from soils and clays by a dithionite-citrate system buffered with sodium bicarbonate. In *Proceedings 7th nat. Conf. on Clays and Clay Minerals, Washington. Committee on clay minerals of the National Academy of Sciences-National Research Concil*, Washington, USA, 317–327.

Metzen, D., Sheridan, G. J., Benyon, R. G., Bolstad, P. V., Griebel, A., & Lane, P. N. J. (2019). Spatio-temporal transpiration patterns reflect vegetation structure in complex upland terrain. *Science of the Total Environment*, *694*, 133551. https://doi.org/10.1016/j.scitotenv.2019.07.357

Miller, A. J., Amundson, R., Burke, I. C., & Yonker, C. (2004). The effect of climate and cultivation on soil organic C and N. *Biogeochemistry*, *67*(1), 57–72.

Minella, J. P., Merten, G. H., Walling, D. E., & Moro, M. (2012). Using ^{137}Cs measurements and sediment yield monitoring to document catchment-scale sediment dynamics and budgets. In *Chengdu symposium on erosion and sediment yields in the changing environment.* Proceedings of a symposium held at the Institute of Mountain Hazards and Environment, CAS-Chngdu, China, 338–344.

Moore, D. M., & Reynolds, R. C. J. (1997). *X-ray diffraction and the identification and analysis of clay minerals* (2nd ed.). Oxford University Press. https://doi.org/10.1038/srep2653

Oades, J. M. (1989). An introduction to organic matter in mineral soils. *Minerals in Soil Environments*, *1*, 89–159.

Ogle, S. M., Breidt, F. J., & Paustian, K. (2005). Agricultural management impacts on soil organic carbon storage under moist and dry climatic conditions of temperate and tropical regions.

Biogeochemistry, *72*(1), 87–121. https://doi.org/10.1007/s10533-004-0360-2

Quijano, L., Beguería, S., Gaspar, L., & Navas, A. (2016). Estimating erosion rates using 137Cs measurements and WATEM/SEDEM in a Mediterranean cultivated field. *Catena*, *138*, 38–51. https://doi.org/10.1016/j.catena.2015.11.009

Robert, M., & Tessier, D. (1974). Méthode de préparation des argiles des sols pour des études minéralogiques. In *Annales Agronomiques* (pp. 859–882). National Institute for Agricultural Research.

Sherrod, L. A., Dunn, G., Peterson, G. A., & Kolberg, R. L. (2002). Inorganic carbon analysis by modified pressure-calcimeter method. *Soil Science Society of America Journal*, *66*(1), 299–305.

Six, J., Conant, R. T., Paul, E. A., & Paustian, K. (2002). Stabilization mechanisms of soil organic matter: Implications for C-saturation of soils. *Plant and Soil*, *241*(2), 155–176. https://doi.org/10.1023/A:1016125726789

Six, J., Elliott, E. T., Paustian, K., & Doran, J. W. (1998). Aggregation and soil organic matter accumulation in cultivated and native grassland soils. *Soil Science Society of America Journal*, *62*(5), 1367. https://doi.org/10.2136/sssaj1998.03615995006200050032x

Steinhof, A., Altenburg, M., & Machts, H. (2017). Sample preparation at the Jena 14C laboratory. *Radiocarbon*, *59*(3), 815. https://doi.org/10.1017/RDC.2017.50

Stuiver, M., & Polach, H. A. (1977). Discussion reporting of 14 C data. *Radiocarbon*, *19*(3), 355–363. https://doi.org/10.1017/s0033822200003672

Tang, J., & Riley, W. J. (2015). Weaker soil carbon-climate feedbacks resulting from microbial and abiotic interactions. *Nature Climate Change*, *5*(1), 56–60. https://doi.org/10.1038/nclimate2438

Toraya, H. (2016). A new method for quantitative phase analysis using X-ray powder diffraction: Direct derivation of weight fractions from observed integrated intensities and chemical compositions of individual phases. *Journal of Applied Crystallography*, *49*(5), 1508–1516. https://doi.org/10.1107/S1600576716010451

Trabucco, A., & Zomer, R. J. (2018). Global aridity index and potential evapotranspiration (ET0) climate database v2. *CGIAR-CSI – Consortium for Spatial Information*, *10*, m9.

Van Oost, K., Quine, T. A., Govers, G., De Gryze, S., Six, J., Harden, J. W., et al. (2007). The impact of agricultural soil erosion on the global carbon cycle. *Science*, *318*(5850), 626–629. https://doi.org/10.1126/science.1145724

Van Oost, K., Verstraeten, G., Doetterl, S., Notebaert, B., Wiaux, F., Broothaerts, N., & Six, J. (2012). Legacy of human-induced C erosion and burial on soil–atmosphere C exchange. *PNAS*, *109*(47), 19492–19497. https://doi.org/10.1073/pnas.1211162109

Viscarra Rossel, R. A., Lee, J., Behrens, T., et al. (2019). Continental-scale soil carbon composition and vulnerability modulated by regional environmental controls. *Nature Geoscience*, *12*, 547–552. https://doi.org/10.1038/s41561-019-0373-z

Wang, X., Cammeraat, E. L. H., Cerli, C., & Kalbitz, K. (2014). Soil aggregation and the stabilization of organic carbon as affected by erosion and deposition. *Soil Biology and Biochemistry*, *72*, 55–65. https://doi.org/10.1016/j.soilbio.2014.01.018

Wang, X., Sanderman, J., & Yoo, K. (2018). Climate-dependent topographic effects on pyrogenic soil carbon in southeastern Australia. *Geoderma*, *322*, 121–130. https://doi.org/10.1016/j.geoderma.2018.02.025

Wang, Y., Wang, S., Adhikari, K., Wang, Q., Sui, Y., & Xin, G. (2019). Effect of cultivation history on soil organic carbon status of arable land in northeastern China. *Geoderma*, *342*, 55–64.

Wang, Z., Hoffmann, T., Six, J., Kaplan, J. O., Govers, G., Doetterl, S., & Van Oost, K. (2017). Human-induced erosion has offset one-third of carbon emissions from land cover change. *Nature Climate Change*, *7*(5), 345–349. https://doi.org/10.1038/nclimate3263

Wang, Z., Van Oost, K., & Govers, G. (2015). Predicting the long-term fate of buried organic carbon in colluvial soils. *Global Biogeochemical Cycles*, *29*(1), 65–79. https://doi.org/10.1002/2014GB004912

Wang, Z., Van Oost, K., Lang, A., Quine, T., Clymans, W., Merckx, R., et al. (2014). The fate of buried organic carbon in colluvial soils: A long-term perspective. *Biogeosciences*, *11*(3), 873. https://doi.org/10.5194/bg-11-873-2014

Wiaux, F., Vanclooster, M., Cornelis, J. T., & Van Oost, K. (2014). Factors controlling soil organic carbon persistence along an eroding hillslope on the loess belt. *Soil Biology and Biochemistry*, *77*, 187–196. https://doi.org/10.1016/j.soilbio.2014.05.032

Wiaux, F., Vanclooster, M., & Van Oost, K. (2015). Vertical partitioning and controlling factors of gradient-based soil carbon dioxide fluxes in two contrasted soil profiles along a loamy hillslope. *Biogeosciences*, *12*(15), 4637–4649. https://doi.org/10.5194/bg-12-4637-2015

Zhang, S., Li, S., Wu, B., Yan, P., & Wei, X. (2011). Study of soil erosion using ^{137}Cs method in rocky desertification region of northern Guangdong. *Forest Research, Beijing*, *24*(2), 239–246.

Zhao, P., Li, L., Lin, L., Zhai, G., Cruse, R. M., & Wang, E. (2022). Response of surface soil nutrients and organic carbon fractions to tillage erosion vs. water erosion in an agricultural landscape. *Soil Science Society of America Journal*, 1–13. https://doi.org/10.1002/saj2.20461

Zhao, P., Li, S., Wang, E., Chen, X., Deng, J., & Zhao, Y. (2018). Tillage erosion and its effect on spatial variations of soil organic carbon in the black soil region of China. *Soil and Tillage Research*, *178*, 72–81. https://doi.org/10.1016/j.still.2017.12.022

SUPPORTING INFORMATION

Additional supporting information can be found online in the Supporting Information section at the end of this article.

How to cite this article: Zhao, P., Doetterl, S., Wang, Z., Hoyt, A. M., Wang, E., Yu, H., Quijano, L., Fallu, D. J., Brown, A. G., Six, J., & Van Oost, K. (2022). Factors controlling SOC stability in colluvial soils under contrasting climate and soil weathering conditions. *European Journal of Soil Science*, *73*(5), e13311. https://doi.org/10.1111/ejss.13311